International Journal of MATERIALS RESEARCH Zeitschrift für METALLKUNDE Original Contributions

C. Aranas Jr. et al.: A metastable phase diagram for the dynamic transformation of austenite above the Ae₃

Clodualdo Aranas Jr., In-Ho Jung, Stephen Yue, Samuel F. Rodrigues, John J. Jonas Materials Engineering, McGill University, Montreal, Canada

A metastable phase diagram for the dynamic transformation of austenite at temperatures above the Ae_3

A method is proposed for calculation of the pseudobinary phase diagram associated with the dynamic transformation of austenite to ferrite. Here the driving force is taken as the difference between the austenite flow stress at the moment of initiation and the yield stress of the fresh Widmanstätten ferrite that takes its place. The energy opposing the transformation consists of the Gibbs energy difference between austenite and ferrite at temperatures above the Ae_3 and the work of accommodating the shear displacements and dilatation associated with the phase change. A metastable phase diagram is calculated for a 0.30 wt.% Mn-0.01 wt.% Si steel by balancing the driving force against the three obstacles. The results show that, under dynamic conditions, the ferrite phase field extends all the way from room temperature to that for the formation of delta ferrite.

Keywords: Dynamic transformation; Austenite; Ferrite; Fe–C phase diagrams; Thermomechanical processing

1. Introduction

In the early work on dynamic transformation (DT), it was shown that DT takes place at temperatures up to $166\,^{\circ}\text{C}$ above the Ae_3 [1, 2]. More recently, this temperature range has been extended to $1350\,^{\circ}\text{C}$, i. e. to $480\,^{\circ}\text{C}$ above the paraequilibrium Ae_3 [3, 4]. The observation that Widmanstätten ferrite [4–7] can be formed throughout the austenite phase field indicates that the conventional Fe–C phase diagram does not apply when austenite is being deformed. It is the aim of this paper

to propose an approach for the derivation of phase diagrams that applies to 'dynamic' conditions and to provide an example of such a diagram for a particular steel.

In order to deal with the effect of deformation on the phases present, three quantities must be evaluated that play particularly important roles, the first of which is totally absent under conventional 'static' conditions. In the latter case, the driving force is the free energy difference between the original and the replacement phase, the latter being of lower energy. In the dynamic case, however, the free energy difference is of opposite sign, so that it becomes a barrier to the transformation instead. Under these conditions, it is the flow stress difference between the work hardened austenite and the much softer ferrite that replaces it that provides the driving force [8, 9].

The other quantities are the work of dilatation and of shear accommodation [10]. Unlike the situation at ambient temperatures, at which these energies are stored elastically, the high temperature versions are not stored reversibly, but involve dissipation by means of plastic work. It is shown below how these three quantities can be evaluated over the experimental temperature range and expressed algebraically. These expressions can then be introduced into the Fe–C database of the FactSage thermodynamic software [11]. A metastable phase diagram is in turn generated employing the modified database and valid over the temperature range and chemical composition range of the experimental data. This type of diagram applies to steel undergoing thermomechanical processing, such as in plate and strip mills [12, 13].

2. The driving force for dynamic transformation

Examples of some Widmanstätten ferrite colonies formed dynamically at temperatures above the Ae_3 are presented in Fig. 1a and b [6]. Their coalescence into polygonal grains is illustrated in Figs. 1c and d. The free energy barrier to their formation is illustrated in Fig. 2 for a 0.06 wt.% C-0.30 wt.% Mn-0.01 wt.% Si steel. It is important to note that this obstacle attains its maximum height at about $1080\,^{\circ}\text{C}$, i.e. about midway between the Ae_3 and the delta ferrite transus.

For the present purpose, it is necessary to add the driving force for the transformation to the Gibbs energy of the austenite, making it more 'unstable' in this way. Here the former is defined in terms of the difference between the austenite flow stress at the DT critical strain and the yield stress of the fresh Widmanstätten ferrite that takes its place [9].

This flow stress difference is converted into units of work done/unit volume by multiplying by unit equivalent strain. Although no formal derivation of this procedure has yet been proposed, this empirical approach is supported by two types of observations. The first involves the displacive transformations that take place during cooling. In this case, the Gibbs energy driving force can be converted into a physically realistic shear stress acting on the habit plane of the transformation by employing a unit equivalent strain of one [14]. The

second class of observation involves dynamic transformations of the type considered here. Under these conditions, an equivalent strain of one is again consistent with the experimental data, as shown below for the present steel, as well as for the other steels that have been examined to date [7].

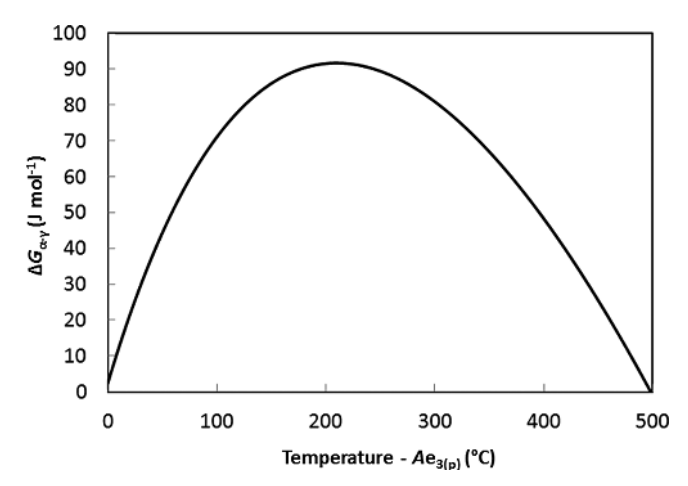


Fig. 2. The chemical free energy difference between austenite and ferrite in the present steel as a function of ΔT (experimental temperature – $Ae_{3(p)}$) [3]. This was calculated using the FSstel database of the Fact-Sage thermodynamic software [11].

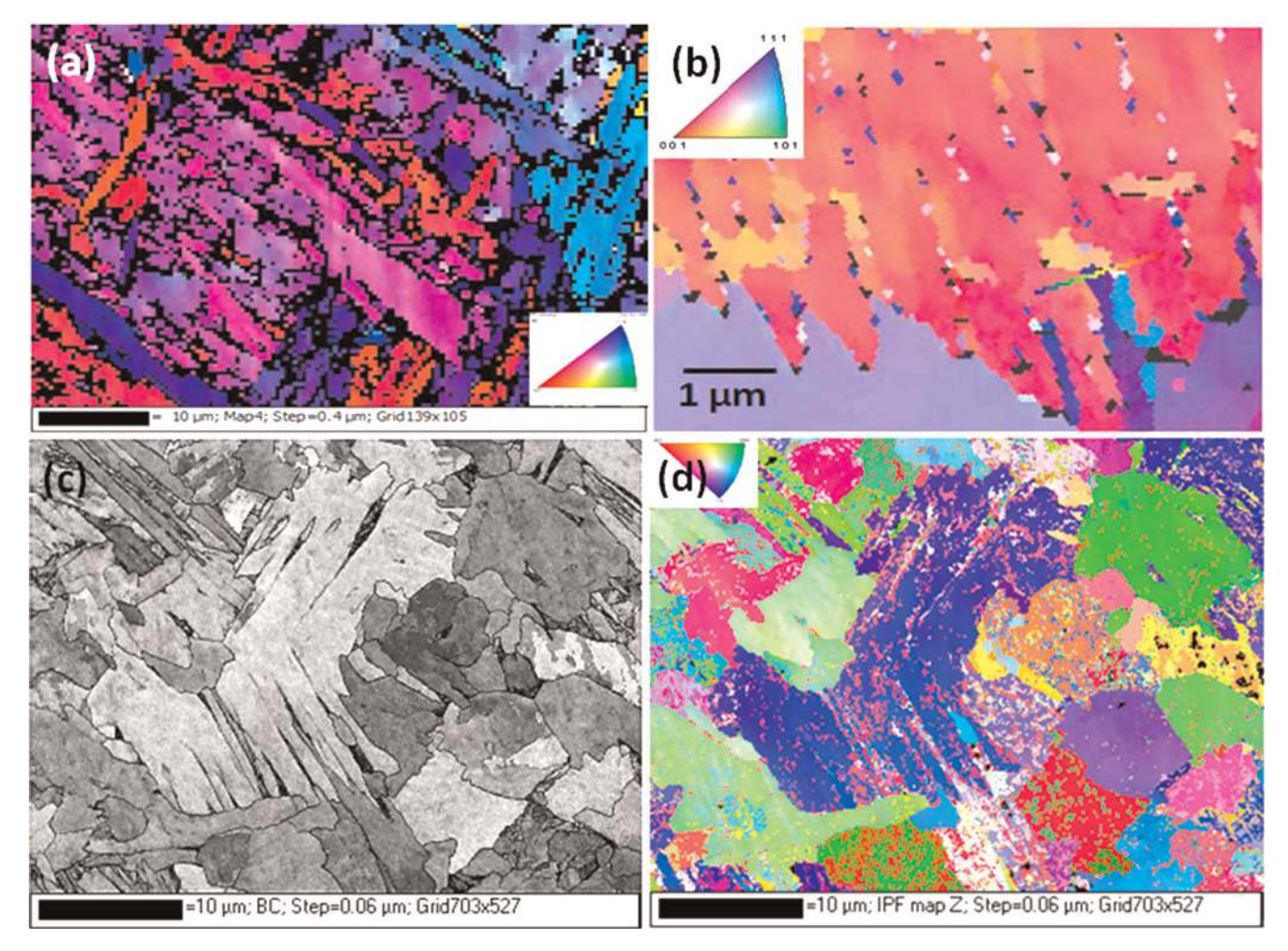


Fig. 1. Colony of Widmanstätten ferrite plates formed dynamically in: (a) a 0.06 wt.% C steel at $1350\,^{\circ}$ C ($Ae_{3(p)} + 480\,^{\circ}$ C) [3], (b) a 0.21 wt.% C steel at $862\,^{\circ}$ C ($Ae_{3(p)} + 40\,^{\circ}$ C) [6], (c) and (d) a 0.06 wt.% C steel at $930\,^{\circ}$ C ($Ae_{3(p)} + 60\,^{\circ}$ C).

The driving force for the present steel was calculated in this way using the data of Refs. [3] and [6] and is illustrated in Fig. 3. Here the critical stresses (σ_c) were determined by applying the double differentiation method to the compression test flow curves at temperatures in the range 920 to $1350\,^{\circ}$ C. These values are plotted against the inverse absolute temperature. For reference, the right-hand axis displays its corresponding value in J mol⁻¹. Note that the work/unit volume differences illustrated here are converted into thermodynamic quantities using the conversion factor 1 MPa = 7.2 J mol⁻¹ [10].

For simplicity, the flow stresses at the melting point were considered here to go to zero, although they actually have small (and unknown) non-zero values at this temperature. The driving force can be seen to be at a maximum in the vicinity of the Ae_3 , but gradually decreases with increasing temperature (i.e. with the decrease in inverse absolute temperature).

The driving forces that can be deduced from Fig. 3 are plotted against temperature in Fig. 4. Here it can be seen that they depend on the Schmid factor applicable to the orientation of the habit plane on which transformation is tak-

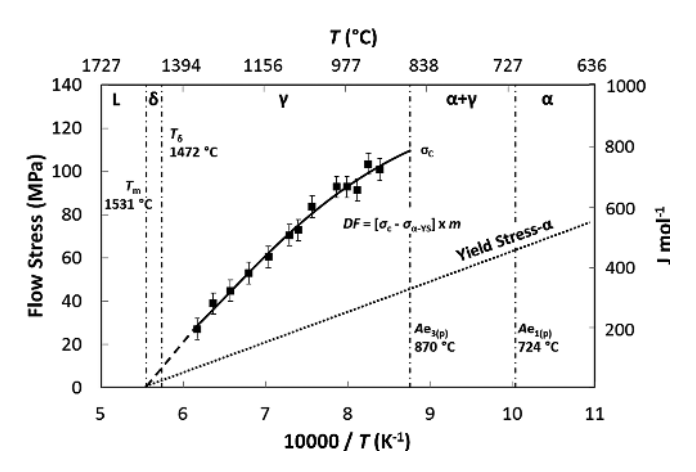


Fig. 3. Effect of temperature on the flow stress at the critical strain in the present 0.06 wt.% C-0.30 wt.% Mn-0.01 wt.% Si steel. The driving force consists of the difference between the critical stress and the estimated yield stress of the fresh ferrite that takes its place. The latter is evaluated by extrapolation from measured values determined below the Ae_1 .

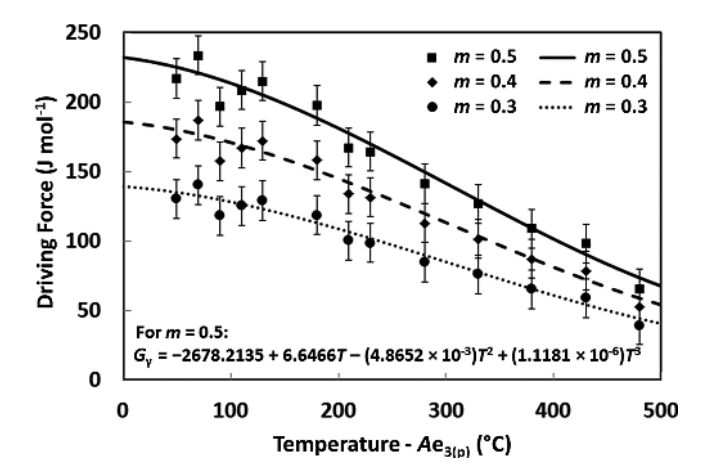


Fig. 4. Dependence of the driving force on temperature and Schmid factor, m. The well-oriented austenite grains (m = 0.5) are subjected to the highest driving forces.

ing place (as well as on the shear direction). For this type of transformation, the habit plane and shear direction were taken to be (0.506, 0.452, 0.735) and (-0.867, 0.414, 0.277), respectively [7]. A Schmid factor of 0.5 corresponds to a particularly well oriented grain, while values of m = 0.4 and m = 0.3 correspond to progressively less and less suitably oriented grains.

In order to incorporate the driving forces of Fig. 4 into the austenite free energy in the Fe–C database of the Fact-Sage [11] or other thermodynamic software, a $3^{\rm rd}$ order polynomial was fitted to the m=0.5 driving force using the OriginPro software. This procedure led to the following equation applicable to the experimental temperature range of $870\,^{\circ}{\rm C}$ to $1\,350\,^{\circ}{\rm C}$:

$$G_{\gamma} = -2678.2135 + 6.6466T - (4.8652 \times 10^{-3})T^{2} + (1.1181 \times 10^{-6})T^{3}$$
(1)

Here G_{γ} is the free energy that must be added to that of the austenite and T is the temperature in Kelvin. That is, this additional mechanical Gibbs energy is simply added to the bulk chemical Gibbs energy of the fcc-Fe. The Fe–C database of the FactSage thermodynamic software was modified by employing this equation to represent the driving force, i.e. the apparent increase in the austenite Gibbs energy.

3. Contribution from accommodation work to the ferrite free energy

The total obstacle to transformation includes the work of shear accommodation and of dilatation, which must be added to the Gibbs energy of the ferrite. The shear accommodation work per unit volume $(W/V)_{SA}$, was calculated here by using the equation [8, 9]:

$$(W/V)_{SA} = m \times \sigma_{c} \times 0.22 \tag{2}$$

Here m is the Schmid factor applicable to the habit plane and shear direction of the transformation, $\sigma_{\rm c}$ is the critical stress required to initiate the phase change, and $\gamma=0.22$ is the shear strain assumed here to be associated with the displacive transformation of austenite to ferrite under the present conditions [7]. The current mechanically-driven phase change is considered in this respect to resemble that of the formation of bainite or acicular ferrite at lower temperatures [7]. Its dependence on temperature is illustrated in Fig. 5a for m values of 0.3, 0.4 and 0.5. The amount of shear work ranges from 25 to 95 J mol⁻¹ for m=0.5 and from 15 to 55 J mol⁻¹ for m=0.3.

The formation of DT ferrite also involves a dilatation strain of about 3%. The work of lattice dilatation per unit volume, $(W/V)_D$, is then given by the equation [9, 10]:

$$(W/V)_{\rm D} = \cos\lambda \times \sigma_{\rm c} \times 0.03 \tag{3}$$

where 0.03 represents the dilatation strain and $\cos \lambda$ is an orientation factor defined as the cosine of the angle between the loading direction and the normal to the habit plane of the transformation. Given that the Schmid factor is defined as $m = \cos \lambda \times \cos \Phi$, here when m = 0.5 and $\lambda = \Phi = 45^{\circ}$, $\cos \lambda = \sqrt{m} = 0.707$. For simplicity, here when m = 0.4 or 0.3, $\cos \lambda$ was set equal to $\cos \Phi$, leading to $\cos \lambda = \sqrt{m} = 0.632$ or 0.548. The dependence on temperature of the dilatation work per unit volume is displayed in Fig. 5b.

This work is significantly less than that for shear accommodation, ranging from 4 to 15 J mol⁻¹ for m = 0.5 and 3 to 13 J mol⁻¹ for m = 0.3.

The sum of the two types of accommodation work is shown plotted against the temperature in Fig. 5c. These dependences were again fitted with a 3^{rd} order polynomial using the OriginPro software. This procedure led to the following equation (for m = 0.5), valid for the temperature range 870°C to 1350°C .

$$G_{\alpha} = -418.83905 + 1.4266T - (1.1594 \times 10^{-3})T^{2} + (2.7756 \times 10^{-7})T^{3}$$
(4)

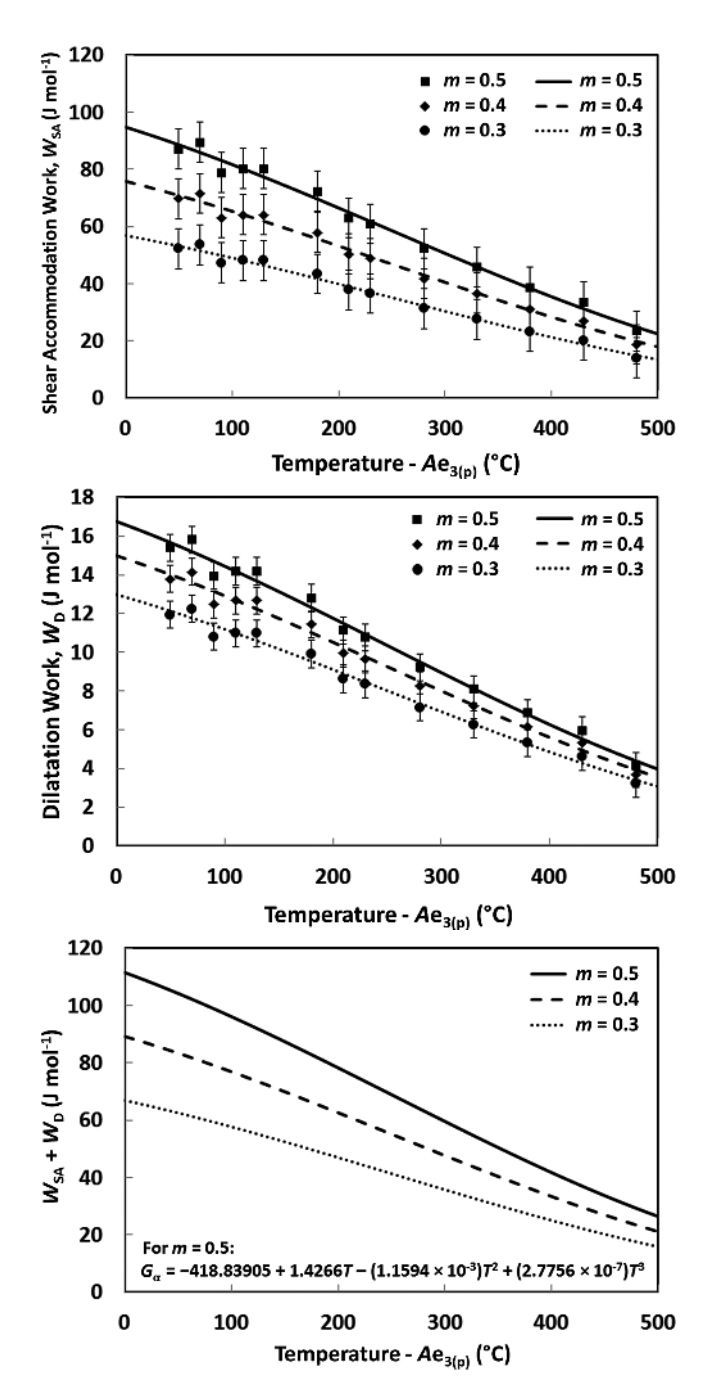


Fig. 5. Dependences on temperature above the Ae_3 of the work of (a) shear accommodation and (b) dilatation. The effect of grain orientation is illustrated by providing curves for m = 0.3, m = 0.4 and m = 0.5. (c) The total accommodation work represented by the sum of Fig. 5a and b plotted against temperature.

This relation was added to the free energy of the ferrite (bcc-Fe), G_a , in the Fe–C database of the FactSage thermodynamic software.

4. Driving force vs total energy obstacles

The total energy obstacle is the sum of the chemical free energy difference between austenite and ferrite and the work of shear accommodation as well as of dilatation during transformation [9, 10]. This is illustrated in Fig. 6 for three values (0.5, 0.4 and 0.3) of the Schmid factor. At around 1040° C, the barrier can be as high as 170 J mol^{-1} for m = 0.5 and around 140 J mol^{-1} , for m = 0.3. As the accommodation work decreases with increasing temperature, the barrier decreases in height to the vicinity of $15-25 \text{ J mol}^{-1}$ at 1350° C.

For comparison purposes, the driving forces of Fig. 4 are plotted together with the total energy obstacle in this figure. It can be seen that the transformation can take place in all well-oriented grains (for which m = 0.5) over the entire temperature range. Here the driving force is always higher than the energy obstacle at the critical strain. Note that the intersections of the driving force and barrier plots determine the maximum temperatures up to which DT can take place (in the model). However, in the case of austenite grains that are not as well oriented (with m = 0.4 or m = 0.3), transformation is not possible at temperatures in the range 130 to 430 °C above the Ae_3 . For these regions to transform, the workpiece must be deformed beyond the critical strain, so that work hardening increases the flow stress and thus the driving force associated with transformation softening.

Another important observation here is that at temperatures close to the formation of δ -ferrite (i.e. above 1 300 °C), the m = 0.4 and m = 0.3 driving forces are higher than their respective obstacles. This means that transformation can take place in this temperature range even in poorly oriented austenite grains.

5. Metastable Fe-C binary phase diagram

It was shown in earlier work [3] that dynamic transformation can be initiated up to 480 °C above the paraequilibrium

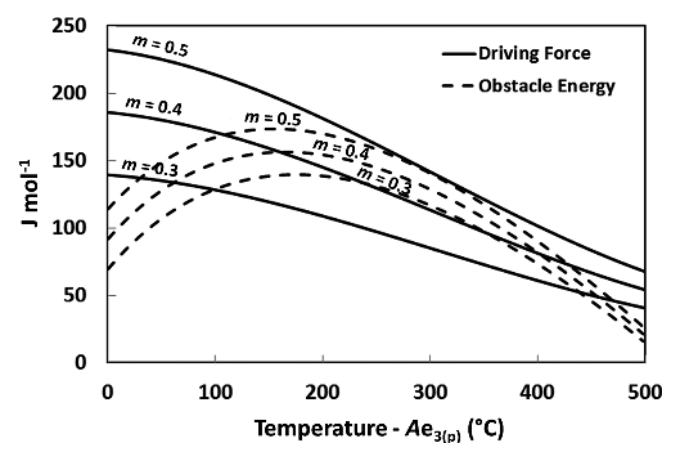


Fig. 6. Dependences of the driving force (solid lines) and total energy obstacle (broken lines) on temperature. The transformation can take place as long as the driving force is greater than or equal to the obstacle height.

Ae₃ temperature. Under these conditions, it is evident that the equilibrium phase diagram for undeformed material does not apply. Such a conventional pseudobinary Fe–C diagram for the present 0.30 wt.% Mn-0.01 wt.% Si steel is illustrated here as Fig. 7a. This was calculated using the FactSage software [11]. It can be seen that ferrite is only stable below about 900 and above 1420 °C. Between these temperatures, only austenite is present. However, this diagram no longer applies when austenite is being deformed because of the dynamic formation of metastable ferrite.

A metastable phase diagram applicable to dynamic transformation can nevertheless be derived, an example of which is presented below. In order to calculate this diagram, the driving force for the transformation must be added to the free energy of the austenite that is specified in the thermodynamic database [11]. In a similar manner, the work of shear accommodation and of dilatation must be added to the Gibbs energy of the ferrite. These quantities have been described algebraically for the present steel in Sections 2 and 3.

The metastable diagram generated with the aid of Fact-Sage software using the Fe-C database modified as de-

scribed above is illustrated in Fig. 7b. Since shear stresses cannot be applied to a sample in the regions containing a liquid (i.e. DT is not possible in this temperature range), the phase boundaries of the L, δ +L and γ +L fields have remained essentially unchanged. A similar concept applies at temperatures below the Ae_1 . Since dynamic transformation cannot be initiated in the absence of austenite, the phase boundaries here still follow those of the conventional Fe–C pseudobinary system. Thus, the metastable phase diagram shown here is only applicable at temperatures between the Ae_1 and the δ and L transus lines.

Note that this diagram only applies to austenite grains with m = 0.5, i.e. to well-oriented grains. This is because the transformation does not occur simultaneously and homogeneously throughout the material, but only in the grains that are appropriately oriented crystallographically with respect to the applied stress. The less well-oriented (lower m-value) grains follow progressively, but require higher and higher levels of flow stress, i.e. of work hardening, before undergoing the phase change. A complete picture of the microstructure then requires knowledge of the volume fractions of the two regions, as this method does

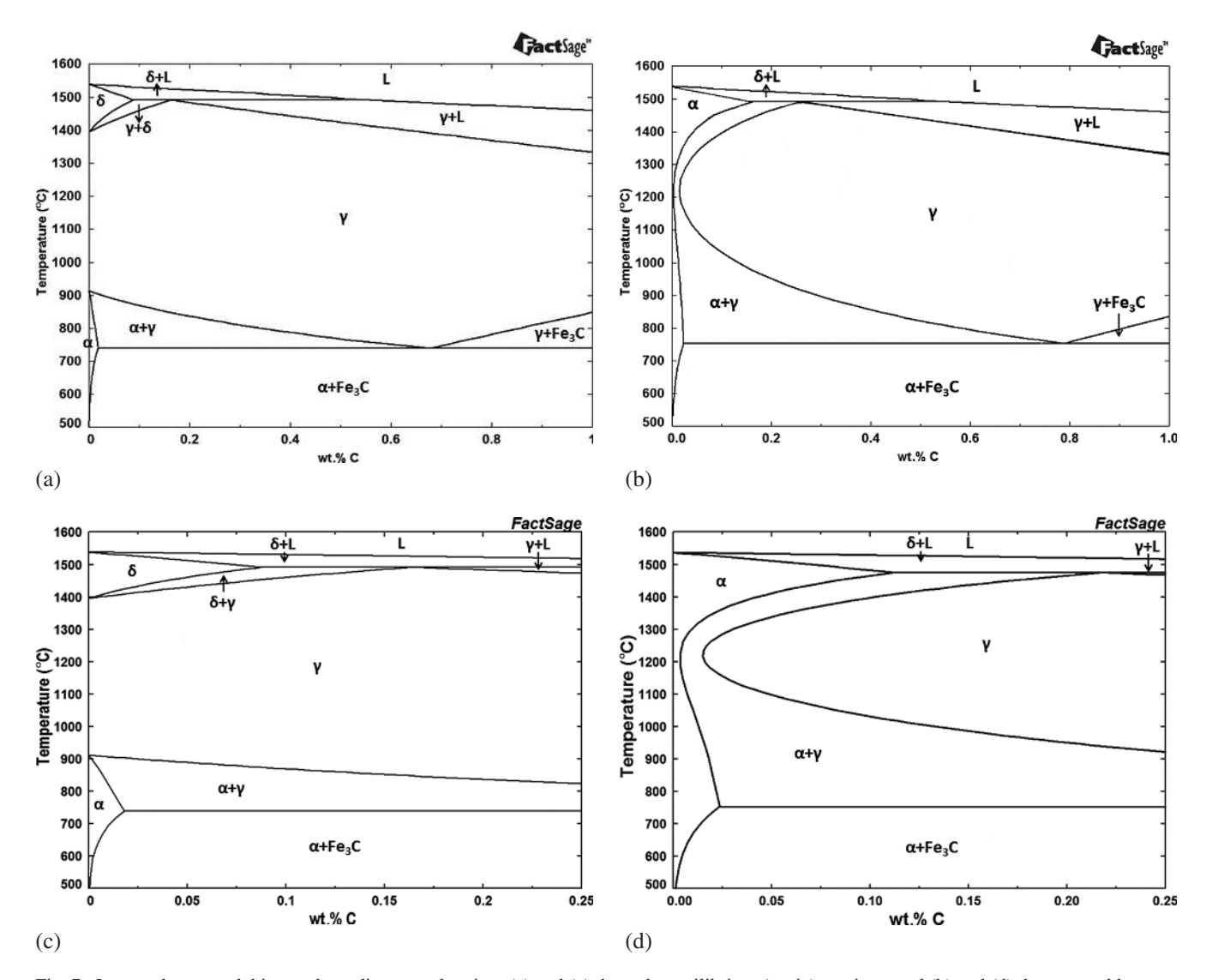


Fig. 7. Iron–carbon pseudobinary phase diagrams showing: (a) and (c) the orthoequilibrium (static) versions, and (b) and (d) the metastable paraequilibrium (dynamic) diagrams applicable to material that has just undergone transformation. Here the single phase α -ferrite domain extends right up to the melting temperature at low C levels.

not lead to the calculation of a composite diagram describing the overall material.

The pseudobinary phase diagram generated here assumes that carbon addition has a negligible effect on the occurrence of DT. This also involves the assumption that the mechanical driving force can be derived in the same way in alloys with different carbon levels but identical amounts of Mn and Si. This view is supported by the observation that dynamic transformation has now been shown to take place in 8 different steels with C levels up to 0.79% (although the Mn and Si concentrations were not held constant in these cases) [5, 6, 8, 9, 15, 16].

As most commercial steels contain only low levels of carbon, the conventional and metastable diagrams of Fig. 7a and b are shown in expanded form in Fig. 7c and d. Here the C level only goes up to 0.25 wt.% C. An important feature of Fig. 7d is that the single phase ferrite region extends right up to the melting point. Concurrently, the single phase austenite field is reduced in size while the two-phase austenite–ferrite region is expanded. It can also be seen here that the solubility limit for carbon in ferrite increases by about 0.03 wt.% at 1480 °C.

6. Conclusions

- 1. The driving force for the transformation, as given by the net softening produced by the phase change, is as high as 230 J mol⁻¹ in the vicinity of the Ae₃ and diminishes gradually to about 20 J mol⁻¹ as the delta ferrite transformation temperature is approached.
- 2. For the case of a 0.06 wt.% C-0.30 wt.% Mn-0.01 wt.% Si steel, this driving force can be described by the equation $G_{\gamma} = -2\ 678.2135 + 6.6466T (4.8652 \times 10^{-3})T^2 + (1.1181 \times 10^{-6})T^3$. This expression is valid over the temperature range 870 °C to 1350 °C.
- 3. The work of shear accommodation and of dilatation associated with the phase transformation in the above steel can be described by the equation $G_{\alpha} = -418.83905 + 1.4266T (1.1594 \times 10^{-3})T^2 + (2.7756 \times 10^{-7})T^3$. This expression is also valid over the temperature range 870 °C to 1350 °C.
- 4. A metastable (dynamic) phase diagram applicable to the thermomechanical processing of steels can be derived by adding the above driving force expression to that for the austenite free energy in the database. In a similar manner, the accommodation work expression must be added to that for the ferrite free energy.
- The single phase ferrite region extends right up to the melting point in the metastable phase diagram and the two-phase austenite–ferrite region is expanded considerably.
- 6. The metastable Fe–C diagram derived here is only applicable to the volume fraction of material that has transformed, i.e. to the austenite grains with the highest Schmid factors. The remainder of the material continues to be described by the conventional (static) phase diagram. As straining proceeds, more and more of the material is described by the former diagram and less and less by the latter. During retransformation on isothermal holding, the above trend is reversed until only the static diagram applies.

The authors acknowledge with gratitude funding received from the McGill Engineering Doctoral Award (MEDA) program (CAJr), the Brazilian National Council for Scientific and Technological Development (CNPq) (SFR) and the Natural Sciences and Engineering Research Council of Canada

References

- [1] Y. Matsumura, H. Yada: Transactions ISIJ 27 (1987) 492.DOI:10.2355/isijinternational1966.27.492
- [2] H. Yada, T. Matsumura, T. Senuma: Proc. Int. Conf. on Physical Metallurgy of Thermomechanical Processing of Steels and Other Metals (THERMEC), ISIJ, Japan (1988) 200.
- [3] R. Grewal, C. Aranas Jr., K. Chadha, D. Shahriari, M. Jahazi, J.J. Jonas: Acta Mater. 109 (2016) 23. DOI:10.1016/j.actamat.2016.02.062
- [4] C. Aranas Jr., R. Grewal, K. Chadha, D. Shahriari, M. Jahazi, J.J. Jonas: Proc. Int. Conf. on Solid-Solid Phase Transformations in Inorganic Materials (PTM 2015), Whistler, BC, Canada (2015) 613.
- [5] V.V. Basabe, J.J. Jonas, C. Ghosh: Steel Res. Int. 85 (2013) 8. DOI:10.1002/srin.201200226
- [6] C. Ghosh, V.V. Basabe, J.J. Jonas: Mater. Sci. Eng. A 591 (2014) 173. DOI:10.1016/j.msea.2013.10.077
- [7] C. Ghosh, C. Aranas Jr., J.J. Jonas: Prog. Mater. Sci. 82 (2016) 151–233. DOI:10.1016/j.pmatsci.2016.04.004
- [8] C. Aranas, T. Nguyen-Minh, R. Grewal, J.J. Jonas: ISIJ International 55 (2015) 300. DOI:10.2355/isijinternational.55.300
- [9] C. Aranas Jr., J.J. Jonas: Acta Mater. 82 (2015) 1. DOI:10.1016/j.actamat.2014.08.060
- [10] J.J. Jonas, C. Ghosh: Acta Mater. 61 (2013) 6125. DOI:10.1016/j.actamat.2013.06.054
- [11] C.W. Bale, E. Belisle, P. Chartrand, S.A. Decterov, G. Eriksson, K. Hack, I.H. Jung, Y.Y. Kang, J. Melancon, A.D. Pelton, C. Robelin, S. Peterson: Calphad 33 (2009) 295. DOI:10.1016/j.calphad.2008.09.009
- [12] C. Aranas Jr., T. Wang, J.J. Jonas: ISIJ International 55 (2015) 647. DOI:10.2355/isijinternational.55.647
- [13] C. Aranas Jr., S.F. Rodrigues, R. Grewal, J.J. Jonas: ISIJ International 55 (2015) 2426. DOI:10.2355/isijinternational.ISIJINT-2015 – 320
- [14] C. Aranas Jr., J.J. Jonas: unpublished work.
- [15] C. Ghosh, V.V. Basabe, J.J. Jonas, Y.M. Kim, I.H. Jung, S. Yue: Acta Mater. 61 (2013) 2348. DOI:10.1016/j.actamat.2013.01.006
- [16] J.J. Jonas, C. Ghosh, X. Quelennec, V.V. Basabe: ISIJ International 53 (2013) 145. DOI:10.2355/isijinternational.53.145

(Received April 22, 2016; accepted June 10, 2016; online since July 20, 2016)

Correspondence address

Dr. Clodualdo Aranas Jr. Materials Engineering McGill University 3610 University, Room 2140 Montreal, Quebec, H3A 0C5 Canada

Tel.: +15143782563 Fax: +15143984492

E-mail: clodualdo.aranas@mail.mcgill.ca

Web: www.mcgill.ca/materials

Bibliography

DOI 10.3139/146.111415 Int. J. Mater. Res. (formerly Z. Metallkd.) 107 (2016) 10; page 881 – 886 © Carl Hanser Verlag GmbH & Co. KG ISSN 1862-5282